



HAL
open science

Heat management and losses of electrocaloric cooling devices based on electrostatic thermal switches

Lucas Depreux, Morgan Almanza, Nouh Zeggai, Fabien Parrain, Martino Lobue

► **To cite this version:**

Lucas Depreux, Morgan Almanza, Nouh Zeggai, Fabien Parrain, Martino Lobue. Heat management and losses of electrocaloric cooling devices based on electrostatic thermal switches. Applied Thermal Engineering, 2022, pp.118290. 10.1016/j.applthermaleng.2022.118290 . hal-03616477

HAL Id: hal-03616477

<https://hal.science/hal-03616477v1>

Submitted on 22 Mar 2022

HAL is a multi-disciplinary open access archive for the deposit and dissemination of scientific research documents, whether they are published or not. The documents may come from teaching and research institutions in France or abroad, or from public or private research centers.

L'archive ouverte pluridisciplinaire **HAL**, est destinée au dépôt et à la diffusion de documents scientifiques de niveau recherche, publiés ou non, émanant des établissements d'enseignement et de recherche français ou étrangers, des laboratoires publics ou privés.

Heat management and losses of electrocaloric cooling devices based on electrostatic thermal switches

Lucas Depreux^{1,2}, Morgan Almanza², Nouh Zeggai², Fabien Parrain¹, and Martino LoBue²

¹Université Paris-Saclay, CNRS, Centre de Nanosciences et de Nanotechnologies, 91120, Palaiseau, France.

²Université Paris-Saclay, ENS Paris-Saclay, CNRS, SATIE, 91190, Gif-sur-Yvette, France.

ABSTRACT – Electrocaloric cooling is a promising technology that could replace existing vapor-compression technology with lighter and more efficient solid state based devices. Among those, electrocaloric coolers using electrostatic actuation are rising; therefore harnessing their advantages and understanding their shortcomings is still a work in progress. In this paper, we pin down two limitations that stem from a commonly used device design, and we propose a model that takes them into account. The first is due to the displacement of the film, which moves the air around and causes losses. We estimate the air losses through a Poiseuille flow model. The second is related to the non-ideal Brayton cycle the device performs and which results in generating a heat flow opposite to cooling. We estimated the effect of this back-flow on the cold flux using a 2D thermal diffusion model. Ultimately, our results point at several possible improvements for further designs. Among them, a slight reduction of the air pressure in the device looks as a promising solution to reduce air losses.

Keywords – *Electrocaloric, Cooling, Electrostatic Actuator, Viscous losses, Air losses, Heat transfer.*

1. INTRODUCTION

Electrocaloric cooling is a promising alternative to vapor-compression technology [1], as it could pave the way for highly efficient, high cooling-power, solid state coolers. Electrocaloric materials (ECM) [2] undergo an entropy and temperature change under the action of an electric field. Their cooling capability is related to the adiabatic temperature change ΔT_{mat} and to the isothermal entropy change ΔS_{mat} , which occur respectively when an electric field is applied or removed along an adiabatic transformation, or when the material is in thermal equilibrium with a heat reservoir. The temperature-entropy diagram shown in Fig. 1 illustrates these two figures of merit jointly with the Brayton cycle, which is typically used for electrocaloric cooling devices. For terpolymers such as P(VDF-TrFE-CFE), ΔT_{mat} and the heat exchanged along an isotherm $T\Delta S_{mat}$ are around 3.4 K [1] and 4.2 J kg⁻¹ K⁻¹ [3], respectively.

Electrocaloric polymer films are all the more remarkable for two reasons: one is that they are compliant, and the other is that the electrodes that are required to trigger the electrocaloric effect can be much thinner than the material itself. Compliance is important for the thermal switch mechanism: it allows good thermal contact with the reservoir as it will conform to the surface, and it lowers the voltage threshold to move the film. Therefore, ECM films open up new possibilities for the design of electrocaloric coolers. Ma and coworkers [1] explored the potential of films and presented one of the most promising devices to date, in which an electrocaloric-polymer film switches thermal contact with the hot and the cold reservoir using electrostatic forces. They report a coefficient of performance (COP) up to 13, a specific cooling power of 2.8 W g⁻¹ and a working frequency of 0.8 Hz. Their design is based on four distinct electrodes (Fig. 2) : one on each reservoir for the electrostatic actuation, and the two compliant electrodes on top and bottom of the film, which

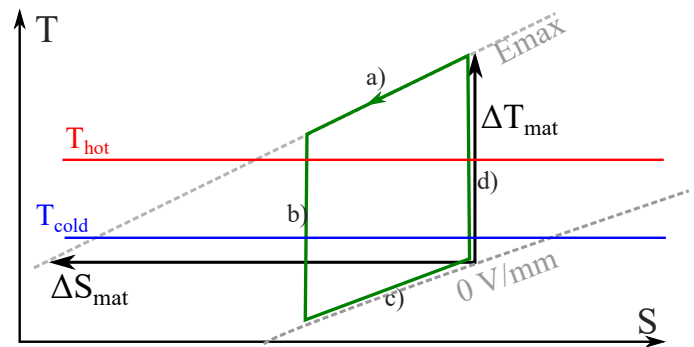


Figure 1. Thermodynamic transformations represented on the temperature-entropy, (T, S) , plane. The grey dashed lines represent two constant electric field transformations of a hypothetical ECM. The isothermal entropy change ΔS_{mat} at a given T , and the adiabatic temperature change ΔT_{mat} at a given S , are represented by the horizontal and vertical black arrows respectively joining the gray lines. A typical Brayton cycle (green lines) is composed by two iso-field transformations taking place in thermal contact with the hot or the cold reservoir (*a* and *c* respectively), and two adiabatic transformations where the field is increased from 0 to E_{max} , or decreased from E_{max} to 0 (*b* and *d* respectively). The red and blue lines represent the temperatures of the hot and cold reservoirs, respectively.

are used both for the actuation and to trigger the electrocaloric effect. During the actuation, the electrostatic pressure attracts the ECM film either towards the hot or towards the cold side, which allows to control the heat transfer. While switching from one contact to the other, the film moves in a zipping-like way through the displacement of an S-shape fold as detailed by Sato et al. [4].

The working cycle of an EC cooler using electrostatic zipping consists of the four steps illustrated in Fig. 2: (a) the film is in contact with the hot side and delivers heat while an electric field is applied to it, (b) while the film is moving under the electrostatic actuation to the cold side for a duration t_{act} , the electric field in the film is removed, which cools it down, (c) the film is in contact with the cold side and absorbs heat and (d) while the film is moving due to the electrostatic actuation to the hot side for a duration t_{act} , an electric field is applied to the film, which heats it up. The working frequency f of the device is the inverse of the time period, t_p , during which the different steps of the cycle are operated.

The adiabatic temperature change of the existing EC materials limits the temperature span of a single stage device to few degrees [2]. The two most explored techniques that overcome this shortcoming are the active regenerator [5], and device cascading [6, 7]. The active regenerator [8] allows to achieve a significant widening of the temperature span using the ECM as a refrigerant and as a heat regenerator at the same time. In this case, the temperature varies along the regenerator, that is from the cold to the hot reservoir, and the heat exchange takes place

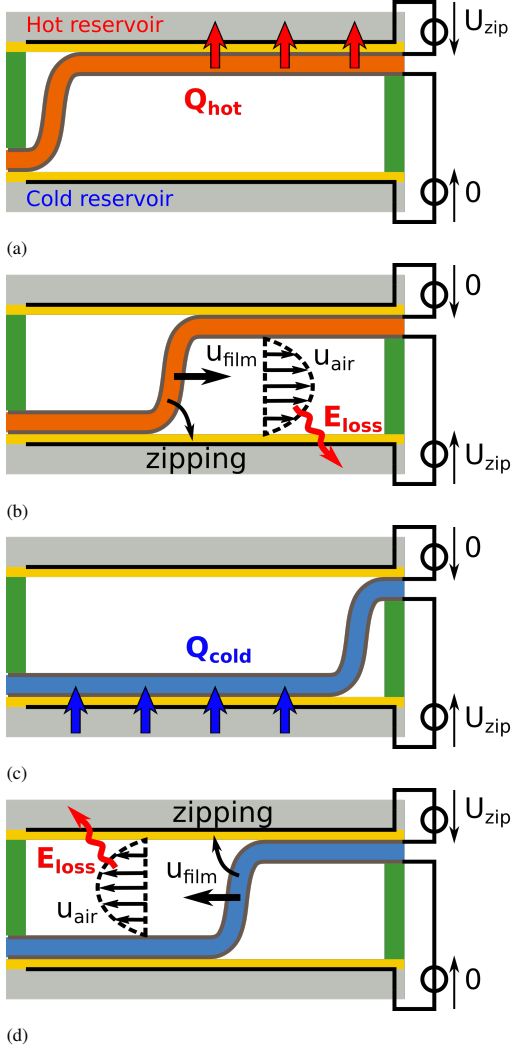


Figure 2. A full cycle of an electrocaloric cooler using electrostatic actuation. The electrocaloric cooling device is based on a thin electrocaloric film, with a layer of metallization on both faces (dark gray lines). These are also used to actuate the film towards the electrodes (black lines) on each reservoir (light gray), using electrostatic forces, the speed of the S-shaped front being u_{film} . On each end, the film is stuck to one of the two electrodes with an insulation layer in-between (yellow), while the electrodes are separated with a spacer (green) of thickness h . When an electric field is applied (orange film in frames (a) and (b)) to trigger the electrocaloric effect, the film is heated and transfers Q_{hot} to the hot reservoir. When the field is removed (blue film in frames (c) and (d)) the film is cooled and receives Q_{cold} from the cold reservoir. u_{air} is the velocity field of the air, and E_{loss} is the energy lost for one actuation.

through a fluid that has to be pumped through the active material.

To circumvent this limitation, one can amplify the temperature span by cascading multiple stages [6, 7]. This cascaded architecture gets rid of the fluids and pumps that are needed in traditional regenerator based designs, and thus it is well-suited for a compact solid-state cooling device. Yet, devices using caloric materials as an active component have so far hardly been able to reach the specific cooling capacity and the COP of vapor-compression technology and heat pumps. Therefore, designing a solid-state heat pump with a high efficiency is a key technological challenge.

Many works focus on improving material properties [2, 9, 10] to increase the temperature span. However, the device must also be carefully designed to take full advantage of the ECM intrinsic properties (i.e. ΔS_{mat} and ΔT_{mat}). Indeed, reaching a high ΔT_{res} requires working closer to ΔT_{mat} , but doing so also lowers the cooling capacity. This is critical for the efficiency of

the device when the cooling capacity reaches the same order of magnitude as the losses caused by the thermal switch. Similarly, increasing the cooling capacity requires to achieve an entropy exchange ΔS closer to ΔS_{mat} or to decrease the exchange time. In both cases, this is possible only if the material gets in good thermal contact with the reservoirs. In brief, the design of a thermal switch presents two major challenges: achieving a good control of the heat transfer, and minimizing the losses due to the switching mechanism.

Although the control of the heat transfer is often what limits the efficiency/power of such devices, recent works on electrostatic based thermal switches [11, 12] have shown that heat management can be carried out very efficiently. Today, the different types of losses of the whole device are still under investigation, and the recent main improvements regarding losses deal with thermal leakage, power electronics for the energy recovery [13, 6] as well as on the EC material. Using well-known methodologies and with an appropriate design, we expect that both thermal leakage and energy recovery can be dealt with. In contrast, modeling material losses and the limitations due to the architecture are still challenges to be met in order to enhance electrocaloric cooling. While electrocaloric materials are a very active field of research [9, 10], the limitations caused by the architecture required to provide a cooling effect have hitherto seldom been addressed in due detail.

Thus, we propose to study the losses of an electrocaloric cooler that uses the zipping actuation mechanism for the thermal switch as shown in Fig. 2.

The actuation losses occur when switching between thermal reservoirs; the ECM film displaces the air around and generates losses because of its friction. As pointed out in the micro electro-mechanical systems (MEMS) literature [14, 15], the air flow might cause serious limitations and energy consumption, and especially when the actuation is fast. Limiting these losses requires a slower actuation. Yet, besides reducing power, slowing down the actuation to decrease the losses gives rise to another drawback. While the field change occurs almost instantaneously through the whole material, the zipping motion is progressive and much slower. Therefore, some parts of the material remain in contact with the wrong reservoir (i.e. with the hot end when the material is cold and vice-versa). This opposite heat transfer, called backflow, degrading the cold flux must be taken into account.

The goal of this work is to study the limitations of the air losses and the backflow in order to provide tools to compare them with other sources of losses. First, we model the air losses using the Hagen-Poiseuille flow model, a quite common first-approximation often adopted in MEMS literature [14, 15]. Next, we introduce the backflow during the displacement of the film. Then, considering the heat diffusion in the film and the backflow, we estimate the cold flux over a thermodynamic cycle and compare it with the losses due to the air flow. Finally, we discuss the possibility of increasing the temperature span ΔT_{res} and getting closer to ΔT_{mat} , which would be more suitable for cooling applications.

2. AIR LOSSES

Due to the film displacement, the air flows between two parallel rigid plates and causes losses, as shown in figure 3. The plates length and width are L and w respectively, and the air can freely enter or exit from both sides of the cavity at $x = 0$ and $x = L$ where the pressure p_{out} is constant. The film thickness is d and the distance between the electrodes is $h + d$. The bent part of the film is located between s and $s + \delta s$, where s changes as the bent part moves from one side to another.

As $d, h, \delta s \ll L$, the S-bend can be approximated with a straight vertical interface located in $x = s$ (viz. the dashed magenta line in Fig. 3) approximating, this way, the bend with a moving piston with both ends opened to the outside. This approximation allows to skip all the interface details related to the

fold shape, focusing on the preponderant volume phenomena associated with the air flow.

When a voltage is applied between one of the two pairs of electrodes, the piston is translated along the x axis with speed u_{film} depending on the applied electric voltage U_{zip} [4]. When the film is zipping from one electrode to the other, the piston pushes the air in front of it, over a distance L , and drags the air behind. Both gas movements can be described as a plane viscous flow. In this study, the air flow along the z axis is not considered.

The most common way of dealing with this state of affairs is to use the parallel plane Hagen-Poiseuille flow model [15], hence we assume the flow to be stationary, unidirectional (along x axis), isothermal, incompressible, laminar and the fluid to be Newtonian. For the operating conditions we consider, the Reynolds number is always below 4000, making the laminar approximation relevant. The Mach number is always below 0.14, which validates the assumption that the flow is quasi-steady, isothermal and that compressibility effects are negligible.

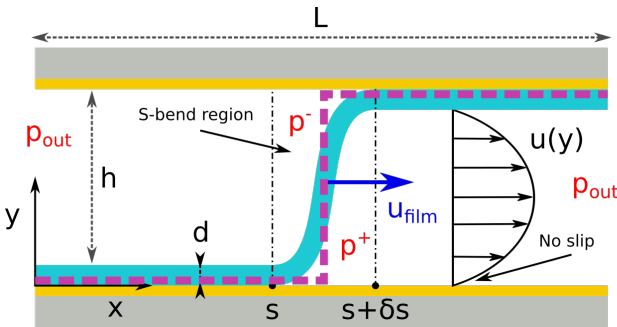


Figure 3. Schematic of the electrostatic actuator during the actuation step (b) in Fig. 2. The polymer film is in cyan, the electrical insulation layer is in yellow, u_{film} is the mean velocity of the film in the x direction. The S-bent region is located between s and $s + \delta s$, and the film is approximated by the dashed magenta line.

The mass conservation under the incompressible assumption gives:

$$\frac{\partial u(x, y)}{\partial x} = 0, \quad (1)$$

where u is the axial velocity of the flow. The force balance equation is:

$$\frac{dp(x)}{dx} = \mu \frac{d^2 u(y)}{dy^2}, \quad (2)$$

where p is the pressure, and μ the viscosity of the air. In order to solve this equation, we need boundary conditions for velocity and pressure. The no-slip condition is generally used for channels assuming $u = 0$ at the walls. By integrating equation (2) along y -axis, where the the velocity profile solution is parabolic, we find the well-known Hagen-Poiseuille equation:

$$\frac{dp(x)}{dx} = \frac{12\mu}{wh^3} D_v, \quad (3)$$

with the flow rate $D_v = whu_{film}$. For instance, when the film moves forward (viz. in the positive x axis direction), it compresses the air in front of it (the air is pushed towards $x = L$) and generates a depression behind it (the air is drained from $x = 0$).

Therefore, we can consider two separate flows: the one in front of the film, $s \leq x \leq L$, and the one behind, $0 \leq x \leq s$, that are connected through the outside pressure p_{out} . By integrating Eq. (3) along x -axis, from s to L and for 0 to s , we have

$$\Delta p = p^+ - p^- = \frac{12\mu L}{wh^3} D_v, \quad (4)$$

where p^+ and p^- are the pressures in front of and behind the film respectively. Eq. (4) shows that the flow generated by the movement of the piston along a distance L is equivalent to the flow in a rectangular pipe of the same length. Now considering t_{act} as the time the film needs to sweep the length L , namely $t_{act} = L/u_{film} = (whL)/D_v$, from (4) we get the following expression for the actuation time:

$$t_{act} = \frac{12\mu L^2}{h^2 \Delta p}. \quad (5)$$

The dissipated power can be written as $\Delta p D_v$, whence the viscous energy loss per actuation $\Delta p D_v t_{act}$ writes:

$$E_{visc} = \frac{12\mu w L^3}{h t_{act}}. \quad (6)$$

As the air is accelerated in the channel, the viscous loss is not the only energy that the actuator must provide. It is worth noting that here we focus on the losses associated with the steady state flow taking into account nothing but the air kinetic energy, namely:

$$K_{air} = \frac{1}{2} (\rho_{air} whL) u_{film}^2 \chi = \frac{3}{5} \frac{\rho_{air} whL^3}{t_{act}^2}, \quad (7)$$

where ρ_{air} is the air density, and $\chi = 6/5$ is the integral of the square of the ratio of the velocity over the mean velocity.

One of the relevant quantities defining the performance of a cooling device is the heat flux through the exchange surface, which is the reason why energies and works are commonly normalized to the surface. Consequently, from here on we shall switch to surface-energies using the plates area $A = wL$ as the normalization factor.

The energy per unit of surface lost due to the viscosity of air is:

$$e_{visc} = \frac{12\mu L^2}{h t_{act}}. \quad (8)$$

Let us consider the worst-case scenario, where the inertia of the fluid is entirely dissipated in the air at each actuation. In the case of a Poiseuille flow, the kinetic energy per unit of surface of the air in the channel is:

$$k_{air} = \frac{3}{5} \frac{\rho_{air} h L^2}{t_{act}^2}. \quad (9)$$

Note that the kinetic energy is proportional to t_{act}^{-2} , whereas the viscous losses are $\propto t_{act}^{-1}$. At high working frequency, the actuation is quicker, and thus the kinetic energy becomes as important as the viscous losses. Considering the total energy loss due to the air,

$$e_{air} = e_{visc} + k_{air} = \frac{12\mu L^2}{h t_{act}} + \frac{3}{5} \frac{\rho_{air} h L^2}{t_{act}^2}, \quad (10)$$

we can find the optimal height h_{opt} by minimizing $e_{air}(h)$,

$$h_{opt} = \sqrt{\frac{20\mu t_{act}}{\rho_{air}}}. \quad (11)$$

Interestingly, the kinetic energy equals the viscous loss at the optimum. The minimized total energy is then,

$$e_{air, min} = \frac{12}{\sqrt{5}} \sqrt{\mu \rho_{air}} \frac{L^2}{t_{act}^{3/2}}, \quad (12)$$

which is the energy dissipated for a single displacement of the film. The total power loss due to air over a period is $2e_{air, min}/t_p$. This is the quantity we shall eventually compare to the device cold flux.

3. NONIDEAL BRAYTON CYCLE: BACKFLOW

During the displacement, one part of the film is in contact with the hot side while the other is in contact with the cold side, yet the field is applied instantaneously over the whole film (Fig. 5 and Fig. 4). Thus, the ECM operates different cycles depending on the position in the film. Because of this, the cycle operated is not an ideal Brayton cycle.

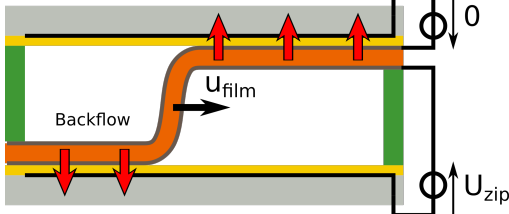


Figure 4. Illustration of back-flow to the cold side when the films moves during step (b).

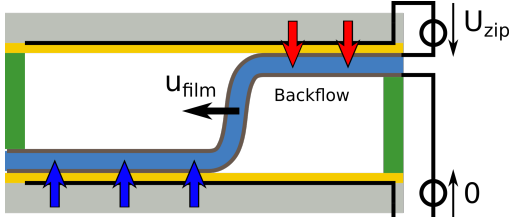


Figure 5. Illustration of back-flow to the hot side when the films moves during step (d).

There are two variables that control the cycle : the electric field applied on the ECM, and the vertical position. As the S-shape actuator is much slower than the electric field change, it is not possible to synchronize the two changes for the whole film. Indeed, while the electric field changes almost instantaneously over the whole film, Eq. (13), each part of the film moves vertically at a different time depending on its position x , Eq. (14).

Therefore, we introduce two more steps in the cycle that occur between the field change and the contact change at a given x . During these steps heat flows in the backward direction, namely from the hot to cold reservoir, and hence we call them backflow steps. To discuss the backflow, we choose to change the field when the film is halfway, that is at $x = L/2$. The backflow steps occur either when the ECM is in contact with the hot side while the field is not applied (Fig. 5), or when the ECM is in contact with the cold one while the field is still applied (Fig. 4).

The electric field is a periodic function defined on the following interval $t \in [0, t_p]$ as follows:

$$E(t) = \begin{cases} E_{max} & \text{for } 0 \leq t < t_p/2 \\ 0 & \text{for } t_p/2 \leq t < t_p. \end{cases} \quad (13)$$

The vertical position y defines which reservoir the film is in thermal contact with. Because the film is considered as a piston, $y(x, t)$ is either 0 or h . In addition, y is a t_p -periodic function which for all $t \in [-t_{bf}(x), t_p - t_{bf}(x)]$ writes,

$$y(x, t) = \begin{cases} h & \text{for } -t_{bf}(x) \leq t < t_p/2 + t_{bf}(x) \\ 0 & \text{for } t_p/2 + t_{bf}(x) \leq t < t_p - t_{bf}(x), \end{cases} \quad (14)$$

where t_{bf} is the algebraic duration of the back-flow step (i.e the delay between the displacement of the film and the electric field change). t_{bf} depends on x and can be either positive or negative depending on the point considered in the film,

$$t_{bf}(x) = \left(\frac{x}{L} - \frac{1}{2} \right) t_{act}. \quad (15)$$

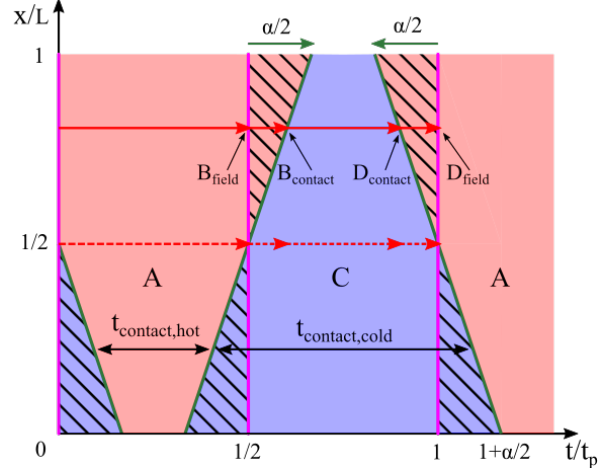


Figure 6. Normalized time duration of the cycle steps depending on the position on the EC film. Step (A) is the exchange with the hot side while the $E = E_{max}$, step (B_{field}) is the field removal, step ($B_{contact}$) is when the film switches position to the cold side while $E = 0$, step (C) is the exchange with the cold side while $E = 0$, step ($D_{contact}$) is when the film switches back to the hot side and step (D_{field}) is when the field is applied.

Figure 6 summarizes the link between the time and the space in relation with the field and the contact change. The magenta lines are associated to the change of field, and, because the field changes at the same time in the whole film, they are vertical lines. On the contrary, the green lines represent the change in thermal contact, and, because of the zipping motion that takes place along the x -axis, they appear as oblique lines whose slope is proportional to the speed of actuation. The hatched area between these lines represents the delay between the field change and the thermal contact change, hence it shows when and where there is backflow. The longer the actuation time t_{act} is, the bigger the hatched area, and the more the cooling flux is reduced. Note that there is only one segment of the film that operates a real Brayton cycle at $x = L/2$ (i.e without back-flow). For $x < L/2$, the film stays in contact with the cold side for too long, whereas for $x > L/2$ it is the opposite.

To minimize the effect of back-flow, the actuation time t_{act} has to be reduced as much as possible. However, as previously shown in equation (12), the air losses increase as t_{act} decreases. This induces a trade-off between the two detrimental effects we addressed here.

4. HEAT TRANSFER MODELING

To estimate the cooling power while taking into account the back-flow, the temperature and the boundary conditions dependence on x must be modeled. The contact with the reservoirs induces a temperature gradient along the film thickness that can be described using a diffusion equation along the y -axis as follows:

$$\frac{\partial T(x, y, t)}{\partial t} = \frac{\lambda}{c} \frac{\partial^2 T(x, y, t)}{\partial y^2} + \frac{\Delta T_{mat}}{E_{max}} \frac{dE(t)}{dt}, \quad (16)$$

with λ the thermal conductivity of the material, c its volumic heat capacity and $E(t)$ the applied electric field. Because of the geometry of the film (i.e. $d \ll L$), the diffusion along the x -axis is negligible. To support this claim, we need first to consider that the film is composed of a thin PVDF based layer ($0.2 \text{ W m}^{-1} \text{ K}^{-1} - 60 \mu\text{m}$) and a gold metallic layer that is even thinner ($320 \text{ W m}^{-1} \text{ K}^{-1} - 10 \text{ nm}$). Note that both layers are important since their conductance is of the same magnitude. The thermal gradient along the x -axis is related to the difference of thermal contact and of the backflow which makes the

cycles slightly different along the x -axis. The former is equal to $(T_{hot} - T_{cold})/h$ and is located in S-bend region of the film, hence it varies in position and time, which leads to a negligible heat flow as it is localized in one spot. The latter leads to a stationary temperature gradient along the x -axis, that is $(T_{hot} - T_{cold})/L$, which induces a negligible heat flow because the conductance along the y -axis is much greater ($d \ll L$). The thermal contact of the film with the hot reservoir at $y = h$ and with the cold reservoir at $y = 0$, is modelled as a linear thermal conductance due to the interface, which corresponds to :

$$\begin{aligned} \lambda \frac{\partial T}{\partial y} \Big|_{y=d} &= -k_i (T(x, d, t) - T_{hot}) (y(x, t)/h) \\ \lambda \frac{\partial T}{\partial y} \Big|_{y=0} &= -k_i (T(x, 0, t) - T_{cold}) (\overline{y(x, t)/h}) \end{aligned} \quad (17)$$

with k_i the interface conductance, T_{cold} and T_{hot} being the temperatures of the cold and hot reservoirs, respectively. The function $y(x, t)/h$ and its complementary $\overline{y(x, t)/h}$ (that are either 0 or 1) define the thermal contact with the hot and cold reservoirs respectively for each slice of the film (along x). When $y(x, t)/h$ equals 1, it is in contact with the hot reservoir, and conversely when it is equal to 0, it is in contact with the cold reservoir. Therefore, when the film is in contact with a reservoir, the flux on the opposite side of the film is necessarily 0.

Finally, the cooling capacity is the heat flux passing at $y = 0$ over a period.

$$q_{cold} = \frac{1}{t_p} \int_0^{t_p} \lambda \frac{\partial T}{\partial y} \Big|_{y=0} dt. \quad (18)$$

To estimate the cooling capacity, a model of the material equation of state reliable over the working temperature range is needed. As the temperature span at half maximum of the ECM entropy/temperature change is above 50 K [3], we can assume the transition to be much wider than the temperature difference between reservoirs. Since the cycle we consider has a small temperature span of 2.5 K, the adiabatic temperature change is almost constant [16] and a linear fit of the entropy s can be considered a rather reliable approximation:

$$s(T, E) = -\frac{\Delta s_{mat}}{\Delta T_{mat}} T - \frac{\Delta s_{mat}}{E_{max}} E, \quad (19)$$

where $\Delta s_{mat} < 0$.

In Eq. (17), it is worth noting that the Robin boundary condition depends on space and time through the temperature, and the contact function. This is why separation of variables, commonly used to solve PDE, is not possible here, and the problem has to be solved numerically. Using a finite volume method, we estimate the average cold flux in a periodic state. Since we focus on how to operate the device, the thermal characteristics of the electrocaloric material and the interface conductance are fixed. For the ECM, we use the properties given in table 1. For the interface exchange coefficient k_i , we use $25 \text{ kW m}^{-2} \text{ K}^{-1}$ [11]. The film thickness is $d = 60 \mu\text{m}$, a typical value in today's prototypes [1, 6, 7]. Aside from the actuation time, the air losses depend on the length of the film and the pressure. Here, the length is $L = 5 \text{ cm}$, and the device is at ambient pressure. Finally, the temperature difference between the reservoirs is $\Delta T_{res} = 1.4 \text{ K}$, and 3.1 K (0.41 and 0.91 of ΔT_{mat} respectively). The former operating point corresponds to Ma's highest COP [1], the latter has been chosen to be closer to the adiabatic temperature change.

Once these values are set, there are still two key parameters that influence the cooling capacity of the device: the frequency f ($1/t_p$), and the actuation time $t_{act} \leq t_p/2$. The working point parametrization can then be quite comprehensively

grasped through two dimensionless variables: $\alpha = t_{act}/t_p$, and $\theta = \Delta T_{res}/\Delta T_{mat}$. The former is a straightforward description of the way changing t_{act} affects the frequency and consequently the power; the latter points at the temperature difference between the material and the reservoirs, describing the average driving force during thermal contact with both ends (i.e. with $\theta \ll 1$ the heat exchange time reduces improving the frequency, with $\theta \equiv 1$ the heat exchange slows down and eventually vanishes).

In Figure 7, we observe that the cooling capacity increases with the frequency. However, two regimes are apparent: on the left side, the power increases linearly as a function of the frequency because a larger number of cycles carrying the same amount of energy are operated per unit of time. On the right side, the power reaches a plateau because the heat transfer is limited either by the diffusion along the film or by the conduction at the interface. We can conclude that to increase the power it is worth to increase the frequency up to 10 Hz, and from there onward, any further increase brings diminished returns.

Furthermore, the power is globally scaled up as θ decreases. Indeed, when reducing θ from 0.91 to 0.41, the increase in the temperature difference between the ECM and the reservoir reduces the heat exchange time, improving the cold flux by the same order due to the linear thermal model.

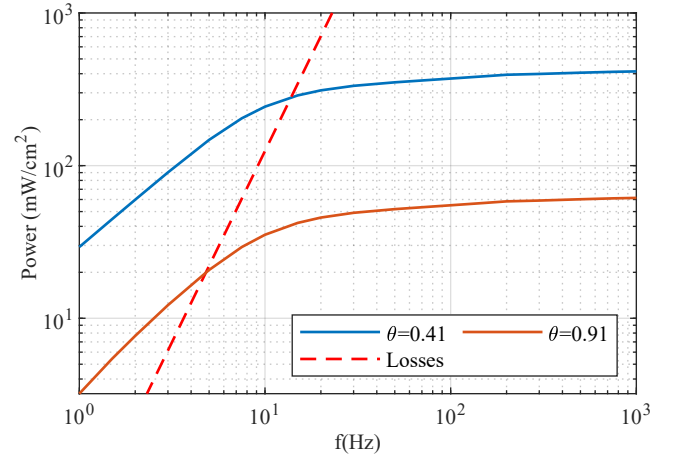


Figure 7. Cold flux function of the frequency with low actuation ratio $\alpha = 0.1\%$ and a temperature ratios of $\theta = 0.91$ and 0.41 ($\Delta T_{res} = 3.1 \text{ K}$, $\Delta T_{res} = 1.4 \text{ K}$).

In practice the temperature ratio θ is related to the environment. Working with high temperature span (high θ) eases the design (less stage and less heat transfer). Therefore, we shall focus next section on the case where $\theta = 0.91$.

The air losses are proportional to $\alpha^{-3/2} f^{5/2}$, as apparent from Eq. (12), and thus they increase as a function of the frequency at a higher rate than the cooling capacity. Fig. 7 makes clear that the air losses and the cooling capacity get within the same order of magnitude at about 4 Hz.

Consequently, to increase the ratio of cooling capacity to losses, and thus the efficiency, the working frequency has to be lower than the 4 Hz. At 1 Hz, the air losses are 10% of the cooling capacity for $\theta = 0.91$. The point with air losses is that they somewhat impose an upper bound on the frequency, and therefore on the cooling capacity output.

Reducing the air losses can be achieved by increasing α , which shifts the dashed line rightwards, as shown in Fig. 8. However, increasing α also amplifies the backflow, which will decrease the cooling capacity, shifting the full lines in Fig. 8 downwards. To get an insight into the losses/backflow trade-off we can follow the cooling capacity, for a given ratio between cooling capacity and losses, as a function of α . The black points in Figure 8 represent the case where the cooling capacity equals the air losses. What's apparent here is that, at fixed loss ratio,

there is a value of α where the cooling capacity reaches a maximum.

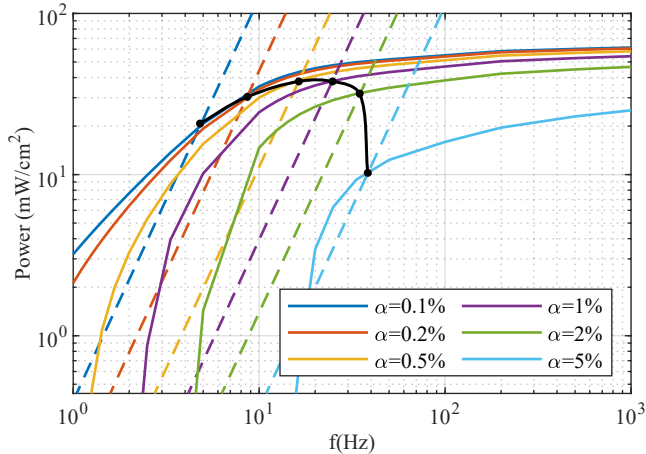


Figure 8. Effect of α on the cooling capacity and on the air losses for a given thickness $d = 60 \mu\text{m}$ and $\theta = 0.91$. The dots correspond to the case where the losses equal the cooling capacity.

To sum up, the losses can be reduced by increasing α , which allows working at higher frequency (higher power), but the trade-off with the back-flow defines an optimal value of α beyond which the cooling capacity quite sharply reduces.

5. DISCUSSION

5.1. Choice of the operating point

The three relevant time scales leading the device are the exchange time τ_{exch} (i.e. the characteristic interval the ECM needs to exchange heat when in contact with the reservoir), the actuation time t_{act} (i.e. related to the zipping speed), and the period t_p (i.e. defining the working frequency). Here we assume all the physical mechanisms underlying τ_{exch} , namely the thermal conductance of the interface k_i , the film diffusivity D , the ECM maximum entropy change ΔS_{mat} , to be fixed according to typical values of state-of-the-art devices [1, 6, 7]. This is the reason why finding the optimum value of α , the ratio between the actuation time and the period, in presence of air losses is the main goal of this work.

If the air losses were negligible (i.e. working under vacuum) the optimum would be keeping α as small as possible. Indeed, a vanishing t_{act} corresponds to an almost instantaneous zipping process with no backflow. Figure 7 shows a similar case, with $\alpha = 0.01$. After a steep power increase as a function of frequency, the cooling capacity reaches a plateau due to the fact that the period becomes too short with respect to τ_{exch} , which wastes the potential of the calorific film. Thereupon, the only way to increase the cooling capacity is to drive a faster heat flow through a larger temperature gradient at the interface, namely reducing θ .

Now, the dashed line in Figure 7 shows air losses calculated through the above presented model. The point where air losses line crosses the cooling capacity function somewhat represents the working frequency upper bound (i.e. the frequency beyond which the cooling capacity equals the losses). As the optimized air losses depends on α as $e_{air,min} \propto \alpha^{-3/2}$, their mitigation can be achieved through the increase of α at the cost of increasing the backflow losses. As a result, the parameter α represents the trade-off between air and backflow losses, which is illustrated in Fig. 8.

Minimizing the losses is paramount for this device, especially because the ECM has a low adiabatic temperature change ΔT_{mat} . This is the major drawback of electrocaloric cooling that can be mitigated by setting ΔT_{res} as close as possible to ΔT_{mat} . However, when ΔT_{res} is high (i.e. when it is close to

ΔT_{mat}), the cooling capacity plummets rapidly, and thus the losses become significant. This underlines the importance of investigating the losses for such a device and finding how to mitigate them. According to our model, the air losses eventually limit the performance of the device, that is both the cooling capacity and the efficiency. To decrease the impact of the air losses, we can increase t_{act} ; this can be achieved either by slowing the frequency or by increasing α :

- When α increases, the air losses are reduced and the back-flow increases. When all the entropy of the film is exchanged, $t_p/2 \gg \tau_{exch}$ (left part of the Fig. 8), even a small α leads to a t_{act} close to τ_{exch} and thus to a drastic power decrease. When only a part of the entropy of the film is exchanged, $t_p/2 \ll \tau_{exch}$ (the plateau in the Fig. 8), larger α are required to have t_{act} close to τ_{exch} and thus the power decreases smoothly.
- Reducing frequency, the air losses are reduced as well as the cooling capacity. Actually, a wise reduction of the cooling capacity represents a way to increase the cooling capacity/air losses ratio. This is the main result of the trade-off between cooling capacity and efficiency studied here.

It is worth noting that, the thermal model presented here reproduces quite accurately the cooling capacity reported in [1, 6, 7]. Ma produces 30 mW cm^{-2} at 1 Hz and $\theta = 0.41$. With a configuration close, Meng single stage provides 70 mW cm^{-2} and 17 mW cm^{-2} for respectively $\theta = 0.41$ and 0.91 . On the contrary, the losses from the electrical power consumed by the actuation reported in [1] greatly exceed our model's estimate, highlighting the need for further experimental investigation.

Ultimately, both losses—air and backflow, have an influence on the COP: as the air losses increase the COP decreases, and the backflow decreases the cooling capacity, which also decreases the COP. Note that the air losses only influence the COP, and have no effect on the cooling capacity, whereas the backflow losses lower the heat absorbed from the cold source, reducing both the cooling capacity and the COP.

5.2. Modeling and assumptions

To evaluate the losses, we focus here on the S-shaped actuation mechanism, yet there is also the possibility to use a U-shaped—as in [11]. The U-shaped mechanism is a bit more complex because the film is first pulled to one of the reservoirs, and once it has collapsed in the middle, the film is zipped in both directions. We opted for the S-shaped mechanism because of its simpler zipping dynamics, and of the opportunity to compare the results with similar architectures presented in the literature.

In this work, thermal leakages have been neglected because we consider the cooling capacity as the primary issue to be addressed. Indeed, the order of magnitude for the cooling capacity is between 10 mW cm^{-2} and 100 mW cm^{-2} , which is larger than the heat flux due to radiation for a few degrees of temperature difference (which is around 0.6 mW cm^{-2} for a difference of 1 K, and assuming that the film has an emissivity of 1). In addition, the use of metal electrodes significantly lowers the emissivity and thus, the radiated power. Furthermore, thermal leakage through the air has been studied in our previous work on the thermal switch [11], showing that it is negligible in the static case. The influence of forced convection has not been mentioned so far in other works, and we guess that their effect is rather small. This is due to the fact that the flow takes place along the x -axis with a non-zero temperature gradient only along the y -axis; thus the convection term in the thermal equation is null. In addition, even if forced convection occurs, it would be during the short amount of time required for the actuation. Finally, the leakage in the spacer can be reduced with an appropriate design, for instance by using thin (small area) and poorly conductive materials.

6. CONCLUSION

To reduce the effect of low adiabatic temperature change, electrocaloric coolers should work with ΔT_{res} close to ΔT_{adia} . However, as ΔT_{res} increases, the cooling power decreases, and thus the losses become preponderant. Therefore, minimizing the losses is mandatory to reach a high temperature span.

The model presented here estimates two sources of power reduction inherent in the above described actuation design: the air losses (kinetic and viscous losses), and the backflow, which is due to the non-ideal Brayton cycle operated in the device. While it is today one of the most promising and studied architectures, this work aims to provide tools to better understand its limitations and to optimize it.

The model can be used to tune the actuation time t_{act} , to find the trade-off between the air losses and the backflow and to optimize the parameter of the device. It is also providing guidelines to improve the device, such as lowering the pressure. For instance, we can quite simply predict that one order of magnitude reduction of air losses can be achieved working under low vacuum (i.e. reducing the pressure to 10 mbar).

Further studies will be devoted to investigate additional loss mechanisms and the possibility of improving the cooling capacity by increasing the film thickness (i.e. introducing a trade-off between power and diffusivity). Indeed, a thicker film carries more heat, hence it increases the power as long as it does not affect the heat transfer. It is also worth noting that a relevant part of the air losses computed here consist of kinetic energy (i.e. a reversible energy term) that, through some design improvement, could be partially recovered. For sure, beyond theoretical modeling, detailed experimental characterization of the different energy terms will be of the utmost relevance for any future advances.

7. ACKNOWLEDGMENTS

This work has benefited from the financial support of the LabEx LaSIPS (ANR-10-LABX-0032-LaSIPS) under the "Investissements d'avenir" program (ANR-11-IDEX-0003) and from (ANR-20-CE05-0044), which are both managed by the French National Research Agency.

8. BIBLIOGRAPHY

- [1] Rujun Ma, Ziyang Zhang, Kwing Tong, David Huber, Roy Kornbluh, Yongho Sungtaek Ju, and Qibing Pei. Highly efficient electrocaloric cooling with electrostatic actuation. *Science*, 357(6356):1130–1134, September 2017.
- [2] X Moya, S Kar-Narayan, and ND Mathur. Caloric materials near ferroic phase transitions. *Nature materials*, 13(5):439–450, 2014.
- [3] Vittorio Basso, Florence Russo, Jean-François Gerard, and Sébastien Pruvost. Direct measurement of the electrocaloric effect in poly(vinylidene fluoride-trifluoroethylene-chlorotrifluoroethylene) terpolymer films. *Applied Physics Letters*, 103(20):202904, November 2013.
- [4] K Sato and M Shikida. An electrostatically actuated gas valve with an s-shaped film element. *Journal of Micromechanics and Microengineering*, 4(4):205–209, dec 1994.
- [5] Uroš Plaznik, Marko Vrabelj, Zdravko Kutnjak, Barbara Malič, Brigita Rožič, Alojz Poredoš, and Andrej Kitanovski. Numerical modelling and experimental validation of a regenerative electrocaloric cooler. *International Journal of Refrigeration*, 98:139–149, February 2019.
- [6] Yuan Meng, Ziyang Zhang, Hanxiang Wu, Ruiyi Wu, Jianghan Wu, Haolun Wang, and Qibing Pei. A cascade electrocaloric cooling device for large temperature lift. *Nature Energy*, October 2020.
- [7] Yiwen Bo, Quan Zhang, Heng Cui, Mengyan Wang, Chunyang Zhang, Wen He, Xiangqian Fan, Yiwen Lv, Xiang Fu, Jiajie Liang, Yi Huang, Rujun Ma, and Yongsheng Chen. Electrostatic actuating double-unit electrocaloric cooling device with high efficiency. page 2003771.
- [8] Uroš Plaznik, Andrej Kitanovski, Brigita Rožič, Barbara Malič, Hana Uršič, Silvo Drnovšek, Jena Cilenssek, Marko Vrabelj, Alojz Poredoš, and Zdravko Kutnjak. Bulk relaxor ferroelectric ceramics as a work-

ing body for an electrocaloric cooling device. *Applied Physics Letters*, 106(4):043903, January 2015. Publisher: American Institute of Physics.

- [9] Guangzu Zhang, Qi Li, Haiming Gu, Shenglin Jiang, Kuo Han, Matthew R. Gadinski, Md Amanul Haque, Qiming Zhang, and Qing Wang. Ferroelectric Polymer Nanocomposites for Room-Temperature Electrocaloric Refrigeration. *Advanced Materials*, 27(8):1450–1454, 2015. _eprint: <https://onlinelibrary.wiley.com/doi/pdf/10.1002/adma.201404591>.
- [10] Florian Le Goupil, Konstantinos Kallitsis, Sylvie Tencé-Girault, Naser Pouriamanesh, Cyril Brochon, Eric Cloutet, Thibaut Soulestin, Fabrice Domingue Dos Santos, Natalie Stingelin, and Georges Hadziioannou. Enhanced Electrocaloric Response of Vinylidene Fluoride-Based Polymers via One-Step Molecular Engineering. *Advanced Functional Materials*, 31(1):2007043, 2021. _eprint: <https://onlinelibrary.wiley.com/doi/pdf/10.1002/adfm.202007043>.
- [11] Morgan Almanza, Lucas Depreux, Fabien Parrain, and Martino LoBue. Electrostatically actuated thermal switch device for caloric film. *Applied Physics Letters*, 112(8):083901, February 2018.
- [12] Hohyun Keum, Myunghoon Seong, Sanjiv Sinha, and Seok Kim. Electrostatically driven collapsible Au thin films assembled using transfer printing for thermal switching. *Applied Physics Letters*, 100(21):211904, May 2012.
- [13] E. Defay, R. Faye, G. Despesse, H. Strozyk, D. Sette, S. Crossley, X. Moya, and N. D. Mathur. Enhanced electrocaloric efficiency via energy recovery. *Nature Communications*, 9(1):1–9, May 2018. Number: 1 Publisher: Nature Publishing Group.
- [14] Mohamed Gad-el Hak. *MEMS: Introduction and Fundamentals*. CRC Press, 1 edition, November 2005.
- [15] Minhang Bao. Chapter 3 - air damping. In Minhang Bao, editor, *Analysis and Design Principles of MEMS Devices*, pages 115 – 174. Elsevier Science, Amsterdam, 2005.
- [16] Xinyu Li, Xiao-shi Qian, S. G. Lu, Jiping Cheng, Zhao Fang, and Q. M. Zhang. Tunable temperature dependence of electrocaloric effect in ferroelectric relaxor poly(vinylidene fluoride-trifluoroethylene-chlorofluoroethylene) terpolymer. *Applied Physics Letters*, 99(5):052907, August 2011.

9. APPENDIX

| Parameter | Value | Description |
|--------------|--|-----------------------|
| L | 5 cm | Channel length |
| ρ_{air} | 1.2 kg m^{-3} | Air density (1 bar) |
| μ | $1.8 \times 10^{-5} \text{ Pa s}$ | Viscosity of air |
| D | $7.8 \times 10^{-8} \text{ m}^2 \text{ s}^{-1}$ | Diffusivity (PVDF) |
| λ | $0.2 \text{ W m}^{-1} \text{ K}^{-1}$ | Conductivity (PVDF) |
| ρ_{ec} | $1.7 \times 10^3 \text{ kg m}^{-3}$ | Mass density (PVDF) |
| c | $1.5 \text{ J kg}^{-1} \text{ K}^{-1}$ | Specific heat (PVDF) |
| k_i | $25 \times 10^3 \text{ W m}^{-2} \text{ K}^{-1}$ | Interface conductance |

Table 1. Parameters used for the simulations.